Dendritic Structure in Lead Crystals Grown from the Melt Using the Seed Crystal (Special Issue on Physics and Inorganic Chemistry)

AUTHOR(S):

Tsujii, Yoshikazu; Maeda, Shigeo; Koyama, Masashige; Takaki, Hideo

CITATION:

Tsujii, Yoshikazu ...[et al]. Dendritic Structure in Lead Crystals Grown from the Melt Using the Seed Crystal (Special Issue on Physics and Inorganic Chemistry). Bulletin of the Institute for Chemical Research, Kyoto University 1966, 44(5): 430-442

ISSUE DATE:

1966-11-15

URL:

http://hdl.handle.net/2433/76138

Dendritic Structure in Lead Crystals Grown from the Melt Using the Seed Crystal

Yoshikazu TSUJII, Shigeo MAEDA, Masashige KOYAMA and Hideo TAKAKI*

(Takaki Laboratory)

Received September 22, 1966

The dendritic structure of cylindrical crystals grown from molten lead by Bridgman method using glass crucibles was examined by the optical microscopy and X-ray method.

At lowering rates of 10 to 50 mm/min, the dendritic structure was observed only around the outside of the samples and the spacing between the primary arms of the dendrites was independent of the lowering rate. But at the inner parts of the samples there occurred transitions from the so-called free dendritic to the cellular dendritic growth and from the cellular dendritic to cellular growth. We have tried to explain these phenomena by the effects of both lateral cooling and unidirectional cooling along the specimen axis. As a second possibility, the above mechanism of growth was also accounted for by the distribution of impurities along a longer axis of a cylindrical section which was analysed spectroscopically.

The relation obtained experimentally by Howarth *et al.* on the aluminum copper alloy, was found to apply in our case.

I. INTRODUCTION

Investigations have been carried out in our laboratory on the substructures in the metal single crystals of tin, nickel and zinc grown from the melt at relatively slow rates of growth[1~5]. Two types of dendritic structures have generally been observed in impure metal crystals grown from the melt: one is "free dendritic" structure, and the other is "cellular dendritic" one. In the latter the temperature gradient in the liquid side of solid-liquid interface is small but positive, so that the latent heat of fusion is conducted into the solid and the rejected solute diffuses into the liquid[6]. In the former, however, the dendritic growth takes place by conduction of latent heat not only into the solid but also into a supercooled melt[6]. Therefore, the cellular dendritic growth in impure metals is, in a sense, intermediate between the free dendritic growth and the cellular one, which is stable to a thin zone of "constitutional supercooling" originating in solute atoms[6].

Tiller *et al.*[7] have shown that the parameter $G/R^{1/2}$ (G, temperature gradient; R, rate of growth) appears to play a similar part in relation to the transition from cellular to cellular dendritc solidification as G/R to the onset of cellular growth. It has, further, been shown by Holmes *et al.*[8] that the critical value of $G/R^{1/2}$ is proportional to C_o/k_o in alloys (C_o, initial solute concentration; k_o, equilibrium distribution coefficient).

As already mentioned, some investigations were carried out in our laboratory on both the cellular structure and the transition from cellular to cellular dendritic

* 辻井芳一, 前田繁男, 小山昌重, 高木秀夫

structure in tin crystals melt-grown from the seed crystals. In these studies, however, the structures were chiefly observed on the outside surfaces of the specimens. A more detailed investigation was carried out on the dendritic structure of lead by using the same methods as in tin. Lead has a simpler structure than tin and has been examined in relatively more detail[9~11].

II. EXPERIMENTAL

Material

The purity of lead used in this study is 99.99%.

Procedures

The crucibles were the glass tubes having elliptical and circular sections at their upper and lower parts respectively, having the conical ends as shown in Fig. 1. Molten lead was sucked up into glass crucibles carefully so as not to produce any cavity as shown in Fig. 1 (a). In this case, the inner wall of crucibles was pre-coated with a paraffin film in order to prevent an interaction between the molten lead and glass[12]. After freezing the molten lead, rod-like seed crystal (99.99% in purity), with the rod axis parallel to [001] (dendrite axis in lead), was put in from the lower end so as to be crystallographically oriented as shown in Fig. 1 (b). Then the crucible was sealed at its lower end and lowered in air in a vertical type electric furnace, the temperature gradient of which was 23°C/

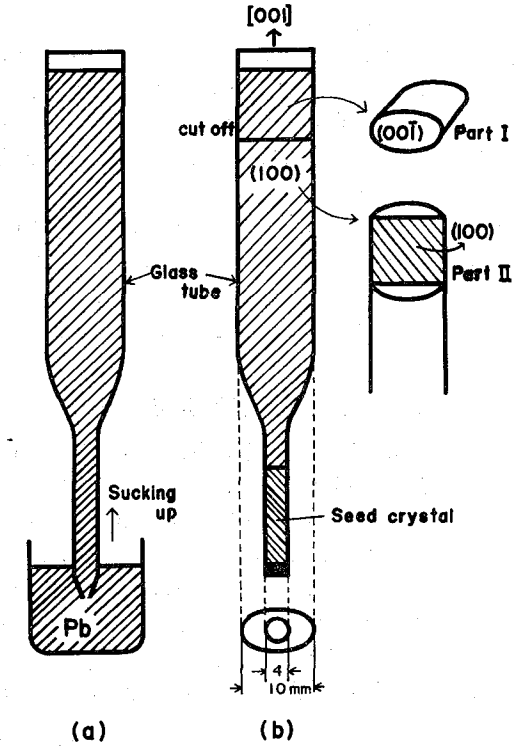

Fig. 1. Crucibles and crystallographic orientations.

cm at 327°C. The lowering rates of 10~50 mm/min were used. After the crystal had been grown, the glass crucible was immersed in a HF solution and removed from the specimen without introducing any mechanical stress. Then the specimen was electro-polished and electro-etched with 60% $HClO_4$ solution at the current densities of 1 and 0.02 A/cm^2.

The structure was examined on the side surfaces of speimen, (100), the sectional surfaces perpendicular to the specimen axis, (00$\bar{1}$), and the longitudinal sections cut along the specimen axis, (100), respectively. The observation of structures was carried out by means of optical microscopy and X-ray diffraction microscopy with CuKα radiation.

III. RESULTS AND DISCUSSIONS

Figs. 2 (a) and (b) show the macro-structure and an enlarged photograph of the side surface (100) of the specimen grown at the lowering rate of 23 mm/min, and Fig. 2 (c) an optical micrograph of the section (00$\bar{1}$) of the specimen**.

Figs. 3 (a) and (b) show the macro-structure and an enlarged photograph of the side surface (100) of the specimen grown at the lowering rate of 41 mm/min, and Fig. 3 (c) an optical micrograph of the section (00$\bar{1}$) of the specimen**.

The dendritic structure, such as shown in Fig. 2 (a) or Fig. 3 (a), was observed in all specimens lowered at rates faster than 10 mm/min. The spacing between the primary arms of the dendrites, however, is independent of the lowering rates as seen in Table 1, in which the relations between the lowering rates and the numbers of dendrites are shown.

The corrugated structure was observed on almost all outside surfaces of the specimens lowered at the rate of 10~11 mm/min, but the dendritic structure developed from corrugations was observed only on the last parts to freeze. The corrugated structure alone was observed in the samples lowered at the rates slower than 10 mm/min.

Howarth and Mondolfo[13] have carried out an investigation in which a series of aluminum copper alloys were cooled unidirectionally at various rates. They have experimentally derived the following relation between the spacing of the dendrite arms (expressed in microns) and the rate of cooling (expressed in deg/sec):

$$S = A \exp (B \cdot \ln R + C \cdot M)$$

where R is the rate of cooling, M the molar fraction of copper, S the spacing of the dendrite arms, and A, B and C the constants.

Measurements were carried out on the spacing of the secondary arms of the dendrites formed on the side surfaces in connection with various rates in the present specimen. The result is shown in Fig. 4. We find a linear relation between the spacing and the lowering rate, provided both coordinates are given in a logarithmic scale. This relation agrees with the above expression if it is assumed that M is equal to zero and R the lowering rate. The constants, A and

** As shown in Fig. 1 (b)-part I, the specimen was cut off at about 15 mm from the upper end of specimen and this section (00$\bar{1}$) was electro-polished and electro-etched.

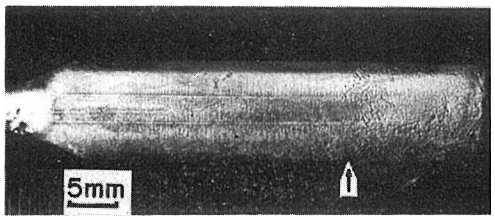

(a)

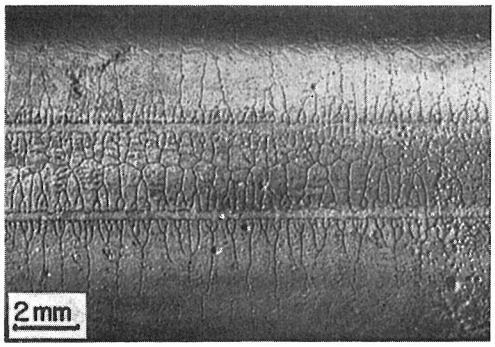

(b)

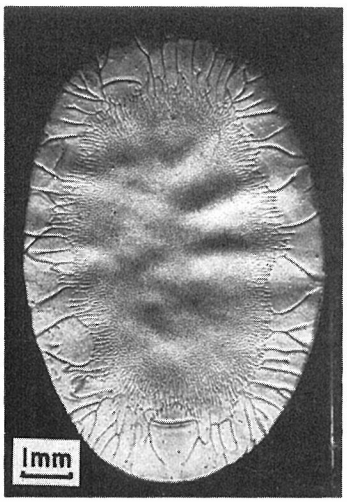

(c)

Fig. 2. (a) Macro-structure of the side surface, (100), of a 99.99% lead crystal grown at the lowering rate of 23 mm/min. (b) Enlarged photograph of a part of (a). (c) Optical micrograph of the transversal section, (00$\bar{1}$), at the part shown with an arrow in (a).

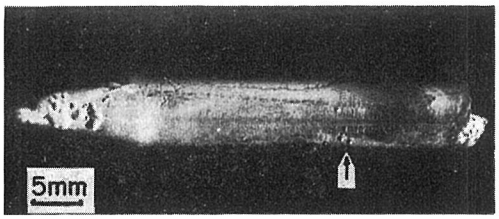

(a)

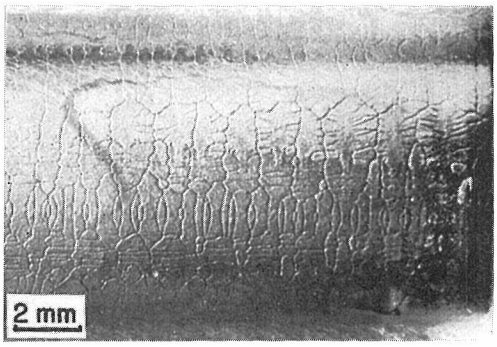

(b)

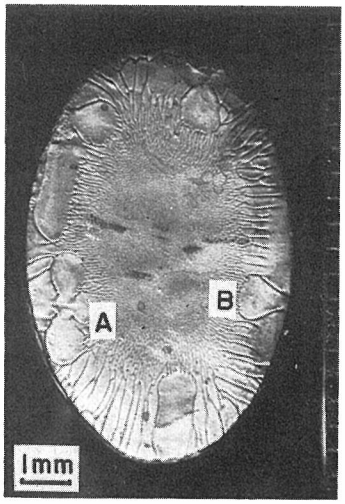

(c)

Fig. 3. (a) Macro-structure of the side surface, (100), of a 99.99% lead crystal grown at the lowering rate of 41 mm/min. (b) Enlarged photograph of a part of (a). (c) Optical micrograph of the transversal section, (00$\bar{1}$), at the part shown with an arrow in (a).

Table 1.

Lowering rate (mm/min)	10	11	13.3	14.2	18.5	19	23	26	31.3	34	41	50.6
Number of dendrite	4	2	5	6	4	6	6	4	5	6	5	4

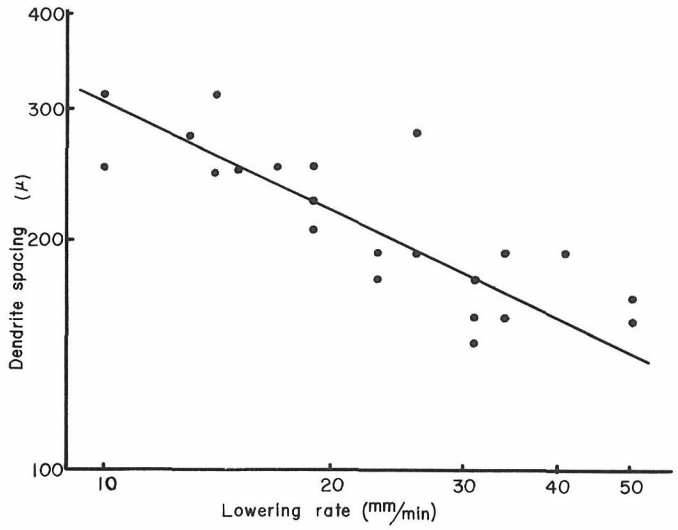

Fig. 4. Spacing of secondary arms of dendrite as a function of lowering rate.

B, evaluated as 1025 and -0.51, respectively.

The dendritic structure is observed only on the outer part of the specimen as seen in Fig. 2 (c) or Fig. 3 (c), but at the inner part of the specimen the cellular structure is always formed. Furthermore, the tertiary arms of the dendrite are observed on the side surface of the specimen, but not on the transversal section. As the lowering rate is incrceased, the region of the dendritic structure on the outside spreads toward the inner direction and the size of cells becomes smaller (see Figs. 5 (a) and (b)).

Figs. 6 (a) and (b) show the enlarged photographs of the dendrites designated with A and B in Fig. 3 (c). The dendrite in this section manifested the shape of a quatrefoil of which the petals spread along the direction of the secondary arms, <100>.

Furthermore at the inner side of each petal, we observed a transition in the type of growth from cellular dendritic to cellular (see Fig. 6 (b)). Another exam-

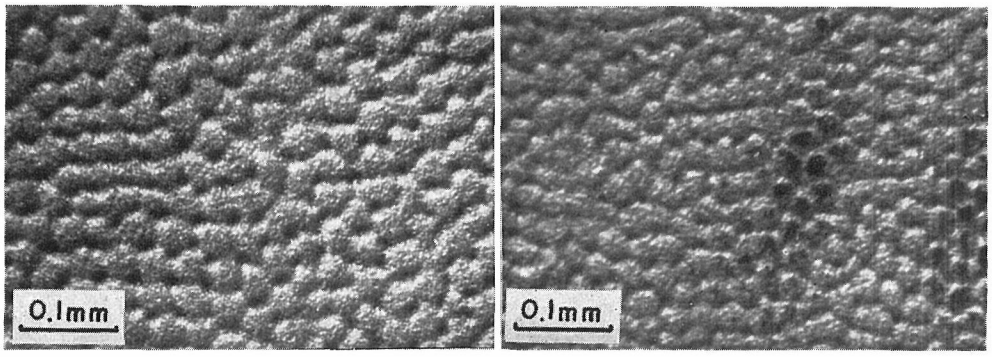

(a) (b)

Fig. 5. (a) and (b) show cellular structures at the central parts in Figs. 2 (c) and 3 (c) respectively.

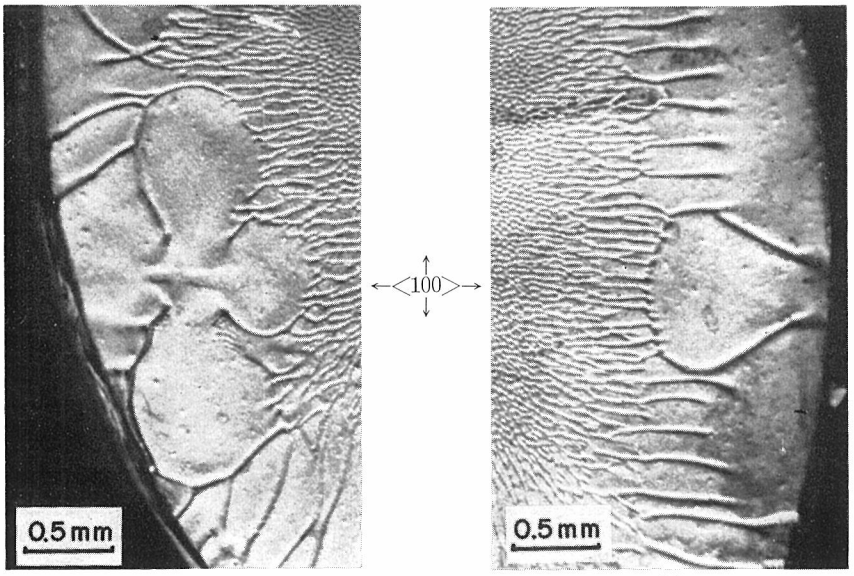

(a) (b)

Fig. 6. (a) and (b) show the enlarged photographs of the dendrites designated with A and B in Fig. 3 (c) respectively.

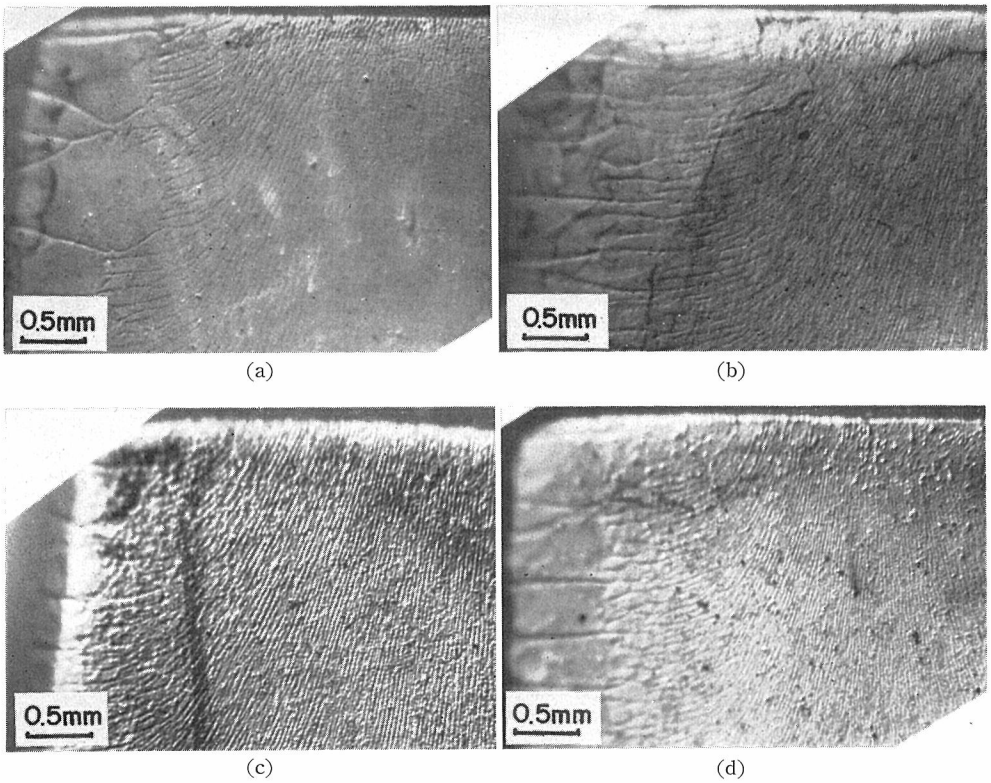

(a) (b)

(c) (d)

Fig. 7. (a), (b), (c) and (d) show the optical micrographs of the longitudinal section, (100), of the specimens grown at the lowering rates of 23, 34, 41 and 50.6 mm/min respectively.

ples of the transition are shown in Fig. 7. These photographs were taken from the longitudinal sections, (100), which were cut along the specimen axes as shown in Fig. 1 (b)-part II. The lowering rates for these specimens were 23, 34, 41 and 50.6 mm/min. The transition of growth form from the secondary arms to the corrugated structure can be seen in this figure. Then the corrugated structure gradually curves in the direction of specimen axis during the growth, and the more rapid the lowering rate becomes the longer the extent of the corrugated structure perpendicular to the specimen axis. The direction of corrugations at the central region, however, is always parallel to the specimen axis.

It is concluded from the above observation that the unidirectional growth in the specimen axis is maintained only at the central region. It is also concluded that heat is transferred toward the side surface at the outside of the specimen because of the relatively small temperature gradient (23°C/cm).

Fig. 8 shows the result of the spectroscopic analysis of some elements in the various parts of the sample, each of which is designated with the numerals, 1, 2,

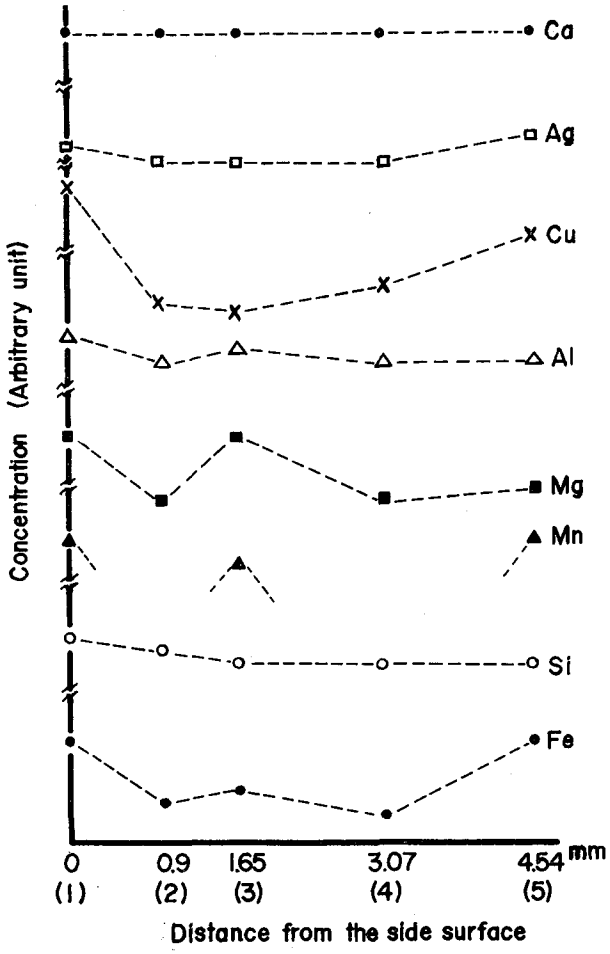

Fig. 8. Result of spectroscopic analysis at the parts designated with the numerals, 1, 2, 3, 4 and 5 in the transversal section. $(0\bar{0}1)$, of Fig. 9.

3, 4 and 5 on the transversal section of the specimen** shown in Fig. 9 (the lowering rate was 34 mm/min)***. The distribution coefficients for most of the elements detected in this analysis are smaller than unity. The concentration of most impurities is high at the surface and decreases with increasing distance from the surface, then increases again. This phenomenon is not explained by the general considerations of dendritic solidification but it is assumed that the following explains the results.

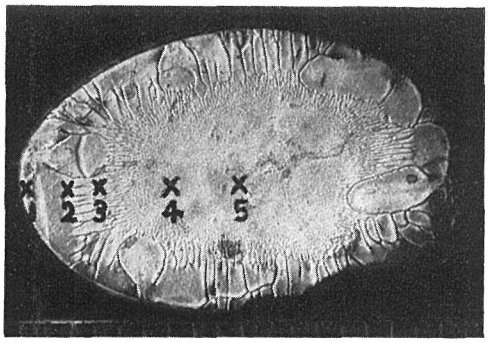

Fig. 9. Optical micrograph of the transversal section, $(00\bar{1})$, of the specimen shown in Fig. 7 (b).

At the faster lowering rates the outer part of the spacimen may be cooled more rapidly. Therefore the primary arms of the dendrites may grow into the supercooled liquid, but the supercooled region may be eliminated by the evolution of latent heat from the pimary arms. On the other hand, constitutional supercooling region may be formed ahead of the primary arms as the result of the impurity accommodation. The inner part of the specimen, however, may still be in the liquid state and the temperature may be higher than that of the primary arms. Accordingly, the temperature gradient from the primary arms toward the liquid may be positive. So, the transition of growth form may occur from the primary arms toward the cellular dendritic secondary arms. The impurity concentration of the frozen solid may be higher in this case because of the larger zone of constitutional supercooling. This consideration agrees with the result of the higher concentration of impurities at the position (1) in Fig. 8. Now the temperatures of the specimen surface, the solid-liquid interface and the inner part of the specimen, T_S, T_I and T_L, will be assumed to be constant as shown in Fig. 10. Fig. 10 is the relation between the distace from the side surface of the specimen and the temperature of the specimen. In this figure the onset of the growth of cellular dendritic secondary arms corresponds to the position 1. The temperature gradient in the solid, however, may be smaller and that in the liquid larger as the cellular dendritic growth of secondary arms proceeds as shown at the positions 2 and 3 in Fig. 10. Accordingly the zone of constitutional supercooling may be thinner so that further transition of growth form may occur from the cellular dendritic to the cellular. In this case, the impurity concentration of the solid will be lower because of the thinner zone of constitutional supercooling

*** The shaving from a drill 0.5 mm in diameter were used for the spectroscopic analysis.

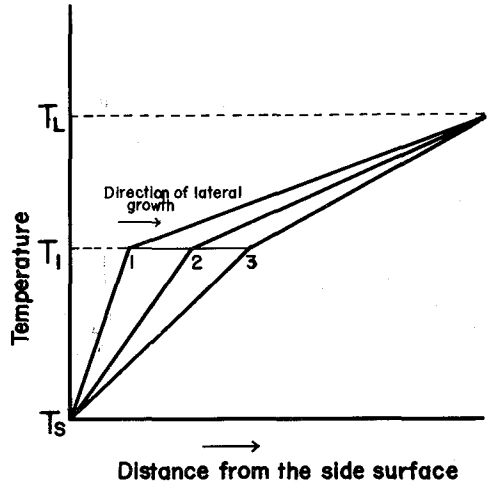

Fig. 10. Relationship between distance from the side surface and temperatures of liquid, interface and solid, T_L, T_I and T_S.

mentioned above. This result also agrees wih the lower concentration of impurities at the position (2) in Fig. 8. As already mentioned, the temperature gradient in the liquid may become larger and that in the solid smaller as the growth proceeds inward. Therefore the actual growth rate may decrease. Cellular growth may be possible despite of the increase of impurity concentration C_0 at the inner part of the specimen, as seen in Fig. 11, where the C_0-$G/R^{1/2}$ diagram derived experimentally on lead tin alloys by Tiller *et al.*[14] is shown. The average concentration of impurities in the solid, however, may be gradually higher as the growth proceeds, because of the rejection of impurities toward the liquid as shown at the inner part of the specimen in Fig. 8.

Fig. 12 (a) shows two Berg-Barrett photographs (reflected from (402)) which were taken from the surface of the specimen in Fig. 2 (b). Then Fig. 12 (b) shows a set of Berg-Barrett patterns which were reflected from $(02\bar{4})$ plane in the section shown Fig. 2 (c)****. Fig. 13 (a) shows two Berg-Barrett photographs which were taken from the specimen surface shown in Fig. 3 (b). Fig. 13 (b) shows two Berg-Barrett photographs which were reflected from $(02\bar{4})$ plane in the section shown in Fig. 3 (c). For example, the regions which are designated with the numerals in Fig. 12 (a) correspond to those designated with the same numerals in Fig. 12 (b) respectively. As seen from Table 1, six denrites are generated around the outer part of this specimen. The Berg-Barrett patterns taken from the transversal section of this specimen are also divided into six regions. Therefore, it seems that the six dendrites initially formed around the outside behave as the centre of further growth.

The boundary between the regions 2 and 3 in Fig. 12 (a) is serrated in shape. This boundary is formed at a place where both side arms of the neighboring

**** In this figure, a series of Berg-Barrett photographs taken from the different parts on the section are patched together.

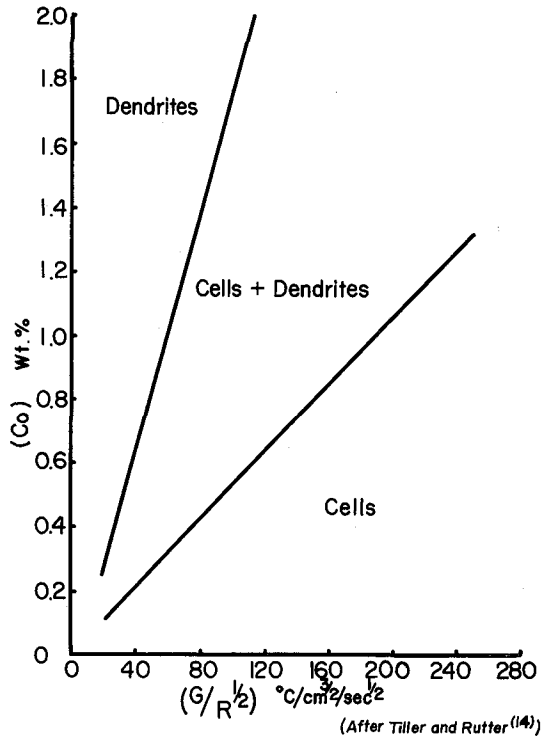

Fig. 11. Effect of growth conditions upon the transition from a cellular to a dendritic interface.

dendrites meet each other. The misorientation of this boundary is about one degree of arc around axes parallel and perpendicular to the specimen axis. A similar result to that mentioned above was also seen in the specimen shown in Fig. 3.

Prohászka[15] has reported a mechanism for the formation of dislocations during dendritic growth. Using the consideration that the temperature of the still growing dendritic branch is always lower than the temperature of another one which has already been formed and is only increasing in tickness, he has shown that the density increases as the square of the temperature difference between the two dendritic branches. In our experimental result, however, no conspicuous misorientation is observed between the neighboring side arms of the dendrite. Therefore, it seems that the relatively large misorientation between the neighboring dendrites is related to the dislocations induced by the segregate impurities between them.

ACKNOWLEDGEMENT

The authors wish to express their best thanks to Mr. T. Sonoda, Department of Metallurgy, Faculty of Engineering, Kyoto University, for his spectroscopic analysis of the sample.

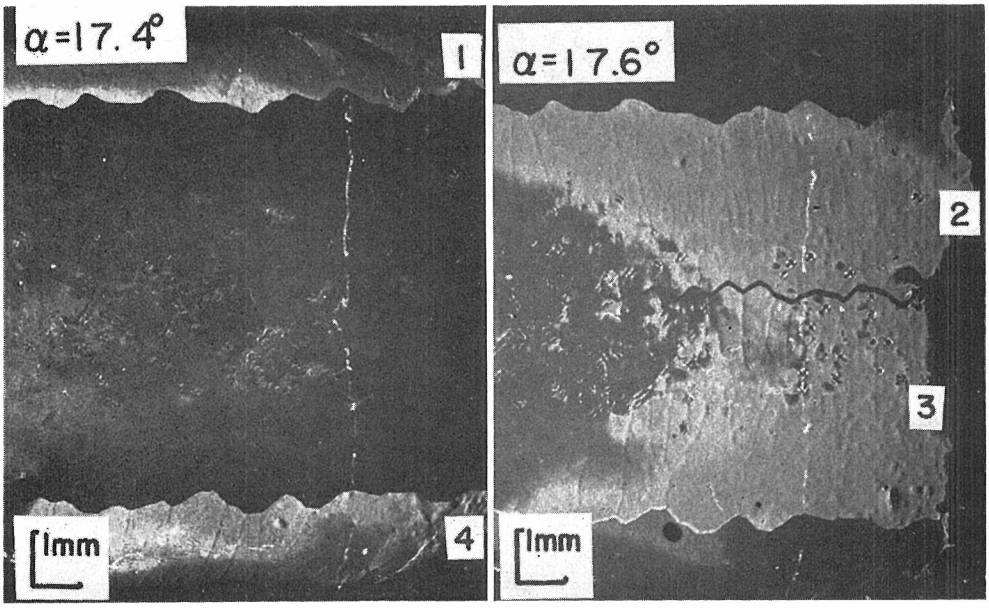

(a)

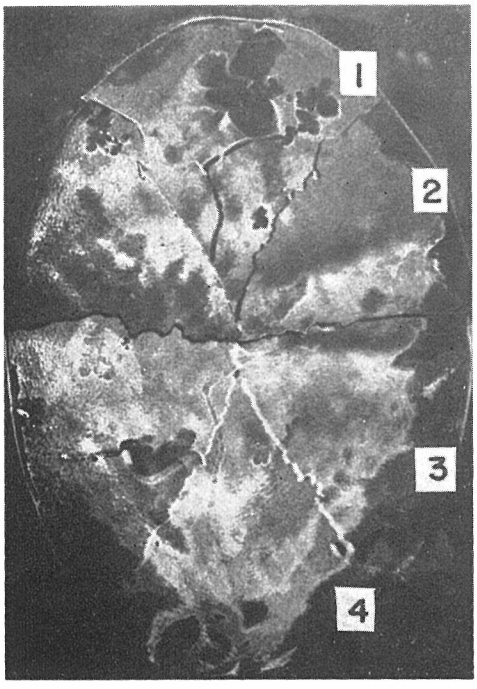

(b)

Fig. 12. (a) Berg-Barrett photographs taken from the side surface of the specimen of Fig. 2 (b). (b) Three pieces of Berg-Barrett photographs taken from the transversal section, $(00\bar{1})$, of Fig. 2 (c).

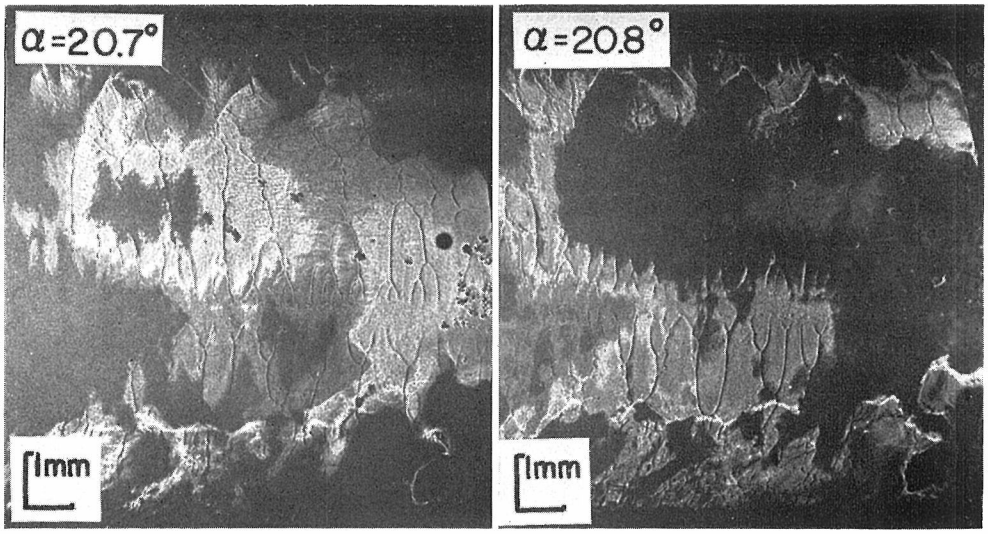

(a)

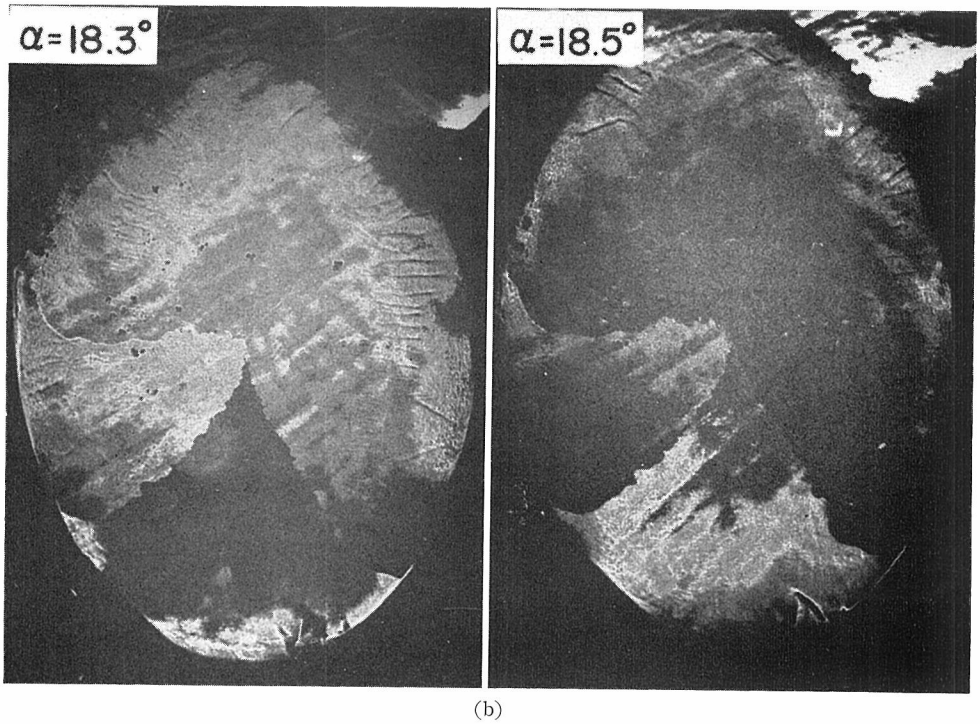

(b)

Fig. 13. (a) Berg-Barrett photographs taken from the side surface of the specimen of Fig. 3 (b). (b) Two Berg-Barrett photographs taken from the transversal section, $(00\bar{1})$, of Fig. 3 (c).

REFERENCES

1) H. Takaki, M. Koyama and H. Fujihira, *J. Japan. Inst. Metals*, **19**, 584 (1955) ; **20**, 266 (1956) ; **21**, 279 (1957) ; **22**, 40 (1958).
2) S. Maeda, This Bulletin, **39**, 278 (1961).
3) M. Koyama, Y. Tsujii and S. Maede, *ibid.*, **42**, 338 (1964).
4) H. Takaki, M. Koyama, Y. Tsujii, K. Iwauchi and S. Maeda, *ibid.*, **43**, 416 (1965).
5) K. Iwauchi, Y. Tsujii, S. Maeda, M. Koyama and H. Takaki, *ibid.*, **43**, 420 (1965).
6) B. Chalmers, *Principles of Solidification*, 103, 164 (1964).
7) W. A. Tiller and J. W. Rutter, *Canad. J. Phys.*, **34**, 96 (1956).
8) E. L. Holmes, J. W. Rutter and W. C. Winegard, *ibid.*, **35**, 1223 (1957).
9) F. Wineberg and B. Chalmers, *ibid.*, **29**, 382 (1951).
10) F. Wineberg and B. Chalmers, *ibid.*, **30**, 488 (1952).
11) T. Orrok (Thesis), *Dendritic Solidification of Metals*, Harvard, 1958.
12) M. Yamamoto and J. Watanabe, *J. Japan. Inst. Metals*, **23**, 675 (1959).
13) J. A. Howarth and L. F. Mondolfo, *Acta Met.*, **10**, 1037 (1962).
14) W. A. Tiller and J. W. Rutter, *Canad. J. Phys.*, **34**, 96 (1956).
15) J. Prohászka, *Acta. Met.*, **11**, 125 (1963).